Kohrangi, M., Kotha, S., Bazzurro, P. (2021): Impact of partially non-ergodic site-specific probabilistic seismic hazard on risk assessment of single buildings. - Earthquake Spectra, 37, 1, 409-427.

https://doi.org/10.1177/8755293020938813

Impact of partially non-ergodic site-specific probabilistic seismic hazard on risk assessment of single buildings

Mohsen Kohrangi, M.EERI[1,2], Sreeram Reddy Kotha[3,4], and Paolo Bazzurro, M.EERI[2]

Abstract
The growth of global ground-motion databases has allowed generation of nonergodic ground-motion prediction equations (GMPEs) based on specific on-site recordings. Several studies have investigated the differences between the hazard estimates from ergodic versus non-ergodic GMPEs. Here instead we focus on the impact of non-ergodic PSHA estimates on the seismic risk of nonlinear single-degree-of-freedom systems representing ductile structures and compare it with the traditional risk estimates obtained using ergodic GMPEs. The structure-and-site-specific risk estimates depend not only on the difference in the hazard estimates but also on the different hazard-consistent ground-motion record selection that informs the response calculation. The more accurate structure-and-site-specific non-ergodic risk estimates show that traditional ones may be biased in a way impossible to predict a priori. Hence, the use of the non-ergodic approach is recommended, whenever possible. However, further advancements of non-ergodic GMPEs are necessary before being routinely utilized in real-life risk assessment applications.

Keywords
Building-specific risk assessment, non-ergodic GMPE, site-specific PSHA, ground-motion selection, ergodic GMPE

Introduction

Ground-motion prediction equations (GMPEs) are widely used in probabilistic seismic hazard assessments (PSHA) to describe the probabilistic distribution of ground-motion intensities at a site from prospective earthquakes in the region. Given the event metadata (magnitude, focal mechanism, etc.) and site metadata (local soil conditions), a typical GMPE predicts not just the median ground-motion intensity level, but also the random distribution of ground-motion intensity that can be expected at the site. The logarithm of an intensity measure (IM; e.g. spectral accelerations or SA, for short) is modeled as a normal random variable $N(\mu, \sigma)$, where μ is the median prediction of the IM and σ quantifies the apparent aleatory randomness of the IM caused by earthquake scenarios of identical parameters. It is well known that s controls the PSHA estimates, especially at very small mean annual rates (MARs) of exceedance of importance for assessing the safety of critical structures. Larger values of σ imply larger values of SAs for the same level of hazard (Bommer and Abrahamson, 2006). With this in mind, efforts are being made to quantify the various contributors to σ (Al Atik et al., 2010); by identifying repeatable effects through analyses of the residual distribution $\varepsilon = N(0, \sigma)$, quantifying and reintroducing the effects into GMPE median as adjustments to the m, and consequently reducing s to a smaller value.

GMPEs should be capable of predicting ground-motion distributions from prospective events of size and location rarely or never occurred in the region around the site of interest. For that purpose, GMPEs are traditionally derived using both physics and statistical regression applied to large datasets of ground-motion

[1] RED – Risk Engineering + Development, Pavia, Italy
[2] IUSS – Scuola Universitaria Superiore Pavia, Pavia, Italy
[3] GFZ German Research Centre for Geosciences, Potsdam, Germany
[4] Universite´ Grenoble Alpes, Universite´ Savoie Mont Blanc, CNRS, IRD, IFSTTAR, ISTerre, Grenoble, France

Corresponding author:
Mohsen Kohrangi, RED – Risk Engineering + Development, Via Frank Giuseppe, 38, 27100 Pavia PV, Italy.
Email: mohsen.kohrangi@redrisk.com

observations compiled from tectonically diverse events recorded at sites scattered across the globe (Akkar et al., 2014b; Ancheta et al., 2014). This practice of substituting temporal samples of ground motion recorded at a single site with ground-motion samples from several sites of similar characteristics is the so-called ergodic assumption (Anderson and Brune, 1999). It has always been clear from its inception that this assumption was a crude approximation but its adoption was simply a necessity. Only recently, with the exponential increase in ground-motion observations at individual sites, it has become possible to quantify and remove one of the variabilities from the apparent aleatory variability s: the site-to-site variability ϕ_{S2S}. Removing ϕ_{S2S} from the σ leads to a dramatic reduction of the ergodic value to that of a single-site value, $\sigma_{SS} = \sqrt{\sigma^2 - \phi_{S2S}^2}$. Using the ϕ_{S2S} of the dataset, for any site with sufficient ground-motion recordings in the dataset, repeatable site-response can be quantified into site-specific random-effect $\delta S2S_S$ - which is a Gaussian random variable with distribution $N(0, \phi_{S2S})$. Along with the single-site aleatory variability σ_{SS}, the values of $\delta S2S_S$ serve as site-specific adjustments, so that the ergodic $N(\mu, \sigma)$ IM predictions for a scenario can be upgraded to partially non-ergodic site-specific predictions $N(\mu + \delta S2S_S, \sigma_{SS})$. Several studies have explored (Rodriguez-Marek et al., 2013; Villani and Abrahamson, 2015) and advanced (Kotha et al., 2017a; Stafford, 2014) the quantification of $\delta S2S_S$ from engineering ground-motion datasets. The impact of using $\delta S2S_S$ to perform site-specific PSHA at several US, European, and Middle-Eastern sites has been evaluated as well (Kotha et al., 2017a; Stewart et al., 2017).

Ongoing studies are focused on compiling much larger ground-motion datasets featuring several hundred sites with enough strong-motion recordings to estimate statistically significant and physically meaningful site-specific $\delta S2S_S$ values (for oscillator periods $T = 0.01 - 10$ s). Of course, in the absence of sufficient site-specific ground-motion data, $\delta S2S_S$ values cannot be reliably estimated and used in site-specific hazard assessment. In such cases, the only alternative is to make ergodic, soil-specific predictions based on-site response proxies in a GMPE, such as time-averaged shear-wave velocity in the top 30 m of soil (V_{s30}).

Clearly, as discussed above, the last few years have witnessed a push toward site-specific PSHA at the regional level. At the same time, in the risk assessment arena research is ongoing to investigate the contribution of hazard uncertainties (Kotha et al., 2018a; Scheingraber and Käser, 2019; Weatherill et al., 2015), significance of local site conditions and site-response proxies (Bazzurro and Cornell, 2004; Rathje et al., 2015; Weatherill et al., 2020), among other aspects, to the uncertainty in the risk estimates. So far, however, to our knowledge no systematic study has been carried out on the impact of partially nonergodic site-specific or non-ergodic PSHA (from hereon) refinements on risk estimates, specifically with the use of empirical site-specific hazard assessment via $\delta S2S_S$. This is the objective of this study, in which we attempt to quantify the impact on risk estimates moving from ergodic to site-specific non-ergodic PSHA. To this end, we select three sites with multiple strong-motion recordings in the pan-European RESORCE dataset (Akkar et al., 2014b), with well-constrained $\delta S2S_S$ estimates over $T = 0.01 - 4.00$ s, to perform both ergodic and non-ergodic PSHA. We subsequently compare the risk computed on the basis of these approaches for a suite of nonlinear single-degree-of-freedom (SDOF) systems representing ductile moment frame buildings located at three representative sites.

Ergodic and non-ergodic GMPEs

The largest differences between ergodic and non-ergodic probabilistic seismic hazard estimates are introduced by the differences between the ergodic and the *partially* non-ergodic site-specific GMPEs. The adverb partially is used here because a fully non-ergodic GMPE would be event, path, and site-specific and perhaps even time-dependent. However, deriving a fully non-ergodic GMPE requires an enormous amount of ground-motion data to minimize modeling (epistemic) uncertainties. The limitations of the currently available ground-motion datasets, however, have only made the derivation of region- and site-specific GMPEs possible. Herein, we use the ergodic Bindi et al. (2014) (B14, hereafter) and the partially non-ergodic region- and site-specific Kotha et al. (2016) (hereafter, K16) GMPEs to perform the PSHA that underpins the risk assessment. Both B14 and K16 GMPEs, which are built on the RESORCE ground-motion database, predict the geometric mean of 5% damped SAs of two horizontal components of the ground motions. These two GMPEs use comparable functional forms as described in the following. Equation 1 illustrates the functional form of ergodic B14 GMPE, which is developed to predict SAs over a range of oscillator periods ($T = 0.01$-4.00 s):

$$\ln(SA_{obs})_{e,s} = f_M(M_w) + f_R(M_w, R_{JB}) + f_S(V_{S30}/V_{ref}) + \delta B_e + \delta W_{e,s} \quad (1)$$

In Equation 1, for each T, $\ln(SA_{obs})_{e,s}$, is the natural-logarithm of the observed SA at site s from event e. The fixed-effects terms of Equation 1 are the magnitude-scaling $f_M(M_w)$ as a function of the event's moment magnitude (M_w), the distance-scaling $f_R(M_w, R_{JB})$ as a function of M_w and Joyner–Boore distance defined as the shortest distance from a site to the surface projection of the rupture surface (R_{JB}), and the *linear* site-response scaling $f_S(V_{S30}/V_{ref})$ as a function of (M_w). In the B14 GMPE, $V_{ref} = 800$m/s, which is the lower V_{S30} limit for class A (i.e. "rock sites") in Eurocode8 soil classifications (Code, 2005).

In a mixed-effects formulation of Equation 1, event-specific random-effect δB_e quantifies the average deviation of observed SAs from event e with respect to the GMPE grand median SA predictions for that scenario event (i.e. M_w and R_{JB}). The between-event (event-to-event or inter-event) variability is captured by the random variable $\delta W_{e,s} = N(0, \tau)$, where τ is the so-called between-event standard deviation. The within-event (record-to-record or intra-event) residuals $\delta W_{e,s} = N(0, \phi)$ quantify ground-motion variability caused by event e at site s that is not explained by the mixed-effects, where ϕ is the so-called within-event standard deviation. Essentially, given M_w, R_{JB}, and V_{S30}, irrespective of whether the event and site are located in Italy, Turkey, or elsewhere in the pan-European region, B14 predicts the same ergodic distributions of SAs; $N(\mu, \sigma)$, whose apparent aleatory variability is $\sigma = \sqrt{\tau^2 + \phi^2}$.

Using all the recordings from Italy and Turkey found in the RESORCE dataset, K16 upgraded B14 with region-specific adjustments to obtain the partially non-ergodic region-specific K16 GMPE applicable to different regions in the pan-Europe. In addition, the region-specific K16 GMPE provides the possibility to be further upgraded for several well-recorded sites in Italy and Turkey to a "region- and site-specific" GMPE (Kotha et al., 2017a), with quantification (along with δB_e) of the site-specific random-effects term $\delta S2S_S$. Equation 2 shows the region- and site-specific K16 GMPE as:

$$\ln(SA_{obs})_{e,s} = f_M(M_w) + f_R^{region}(M_w, R_{JB}) + \sigma S2S_S + \delta B_e + \delta W_{e,s} \quad (2)$$

Except for $f_M(M_w)$, K16 differs from B14 in a few aspects: in Equation 2, (1) the $f_R^{region}(M_w, R_{JB})$ is regionalized to account for differences in anelastic distance decay of short-period SAs($T = 0.01$-1.00 s) between Italy, Turkey, and the rest of pan-Europe; (2) while in B14 (Equation 1), the apparent aleatory residuals are split into between-event δB_e and within-event $\delta W_{e,s}$, in K16 they are split into δB_e, the additional between-site $\delta S2S_S$, and event-and-site corrected $\delta W_{e,s}$ residual distributions; and (3) the region- and site-specific K16 predictions make use of the site-specific $\delta S2S_S$ term instead of V_{S30} to reflect both the soil and site effects (i.e. selective amplification/attenuation of SAs over $T = 0.01$-4.00 s), while in the ergodic B14 the SA prediction is a function only of the soil conditions at the site captured by its V_{S30}.

In sum, the B14 GMPE predictions follow the distribution $N(\mu, \sigma)$, where the aleatory variability $\sigma = \sqrt{\tau^2 + \phi^2}$. K16 GMPE's region- and site-specific predictions, however, are characterized by $N(\mu + \delta S2S_S, \sigma_{SS})$, where the aleatory variability $\sigma_{SS} = \sqrt{\tau^2 + \phi_{SS}^2}$ - the between-site variability ϕ_{S2S} is no longer considered as part of the aleatory variability. Needless to say, a reduction in the aleatory variability is accompanied by an increase in epistemic uncertainty, which in this case is the standard error on $\delta S2S_S$ of each site. Reduction in s and increase in epistemic uncertainty have a strong impact on seismic hazard estimates that in turn we expect to have an impact on risk estimates.

Site-specific response spectra

To compare the risk estimates based on ergodic $\delta S2S_S$-based hazard estimates against those computed using the hazard estimates based on the site-specific $\delta S2S_S$ term, the three selected sites are the recording stations labeled "4802", "4401", and "777" in the RESORCE dataset. In this study, these three sites are referred to as Sites #1, #2, and #3, respectively. For each site, RESORCE dataset contains 8–10 ground-motion recordings. With this amount of data per station, K16 estimates $\delta S2S_S$ with reasonably small standard errors. A map showing the location of selected sites and the recorded events is provided in the Supplementary Material.

It is important to note that, since the ground-motion data from these sites and their events is already used in the B14 and K16 GMPE regressions, there is no need to estimate between-event and between-site terms. Usually, for *new* sites and events whose ground-motion data are not included in the mixed-effects regression

Table 1
Three selected sites from RESORCE database

Site #	Station #	V_{S30} (m/s)	Latitude (degree)	Longitude (degree)	N_{obs} [a]	PGA (m/s²)
1	"4802"	747	37.033	27.440	8	0.02-0.22
2	"4401"	481	38.350	38.340	10	0.01-0.18
3	"777"	339	41.020	28.950	8	0.03-1.72

PGA: ground-motion prediction.
[a] The number of observations may decrease when deriving SAs with increasing period T due to the lower bound of the usable frequency ranges of the records.

of a GMPE; one would first have to estimate the total aleatory residuals using an existing GMPE, $\varepsilon^{new} = \ln(SA_{obs})_{e,s}^{new} - \ln(\mu)$, and then split these into between-event, between-site random effects, and residuals, as in $\varepsilon^{new} = \delta B_e^{new} + \delta S2S_s^{new} + \delta W_{e,s}^{new}$, using a mixed-effect algorithm. In such cases, it is necessary that each new event and site is sampled by multiple recordings to ensure that biases in their random-effects are minimized. However, Kotha et al. (2016) adopted the Stafford (2014) procedure of estimating $\delta S2S_s$ while regressing the mixed effects K16 GMPE. The unbiased estimates of $\delta S2S_s$ used in this study can be disseminated upon request. Table 1 lists the available metadata for the three selected sites. Unfortunately, as with most sites in the pan-European region, very limited site characterization information is publicly available.

Figure 1a shows the observed geometric-mean horizontal response spectra at the selected sites, each one normalized by the geometric mean of the corresponding peak ground acceleration (PGA). Figure 1b shows the site-specific term of K16, that is, the median (shown as solid lines) and standard errors of estimation (shown by colored ribbons) of $\varepsilon^{\delta S2S_2}$, at the three sites. The line color scheme selected to distinguish the three sites in Figure 1 is maintained throughout the article.

Site #3 shows an apparent site-specific amplification peak at around $T = 0.5$ s, which is successfully captured by the site-specific term $\varepsilon^{\delta S2S_2}$ of K16, as depicted in Figure 1b. The site-term for Site #2 shows an amplification plateau (with respect to PGA) peaking at $T = 0.2$ s with $\varepsilon^{\delta S2S_2} = 1.25$, and Site #1 strongly attenuates SAs at all spectral ordinates with $\varepsilon^{\delta S2S_2} < 1.0$. The differences observed in the values of the site-term for these three sites can be explained with reference to their V_{S30}, together with some understanding of mixed effects. There are three main aspects.

First, the site terms are produced as site-specific random-effects in the mixed-effects regression of K16,

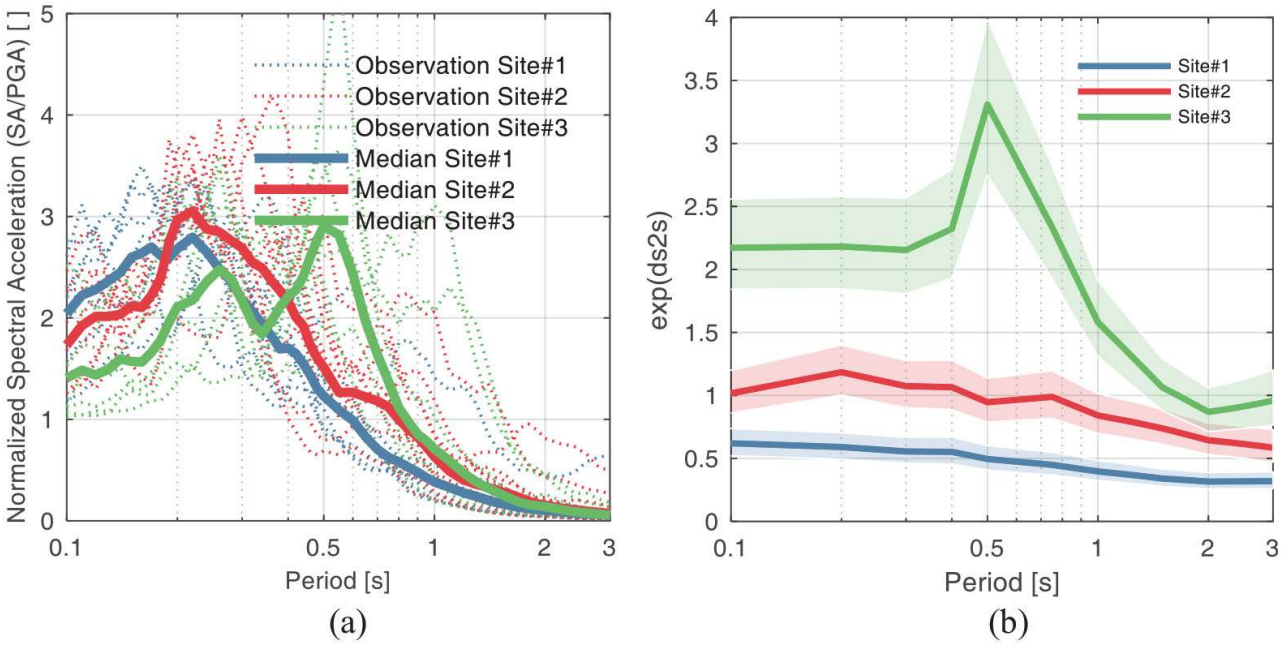

Figure 1. *(a) Plot of the normalized (to PGA) geomean of the response spectra of the horizontal ground motions recorded in the selected sites. (b) Illustration of the median $\varepsilon^{\delta S2S_2}$ values for the selected sites. Dotted lines in panel "b" indicate the uncertainty in estimation of the median $\varepsilon^{\delta S2S_2}$ due to the limited number of records at the site.*

without using V_{S3} (or any site-response proxy) as site-response predictor variable. Therefore, sites that show systematic amplification or attenuation (of SA at a specific T) relative to the average of all sites in the dataset are attributed higher or lower $\delta S2S_s$ values (at T), respectively, regardless of their V_{S3} values. This feature of K16, for example, is clear in the large amplification of SA at $T = 0.5$ s at Site #3.

Second, the RESORCE dataset features a variety of very soft to hard rock sites with $V_{S30} = 100$-1000m/s. The site term, therefore, should be able to reflect the soil conditions of a site in amplifying or attenuating the ground motion. In general, rock sites show strong attenuation with respect to softer sites resulting in a *relatively* lower $\delta S2S_s$ in K16. By inspecting Figure 1b and Table 1, this comment becomes clearer. Because Site #1 is located on rock conditions with $V_{S30} = 747$m/s (i.e. class A of Eurocode 8), the K16 GMPE regression assigns a low $\delta S2S_s$ value at all spectral ordinates of this site. Site #3, on the contrast, is located on stiff soil with $V_{S30} = 339$ m/s (i.e. class C of Eurocode 8) thus relatively higher $\delta S2S_s$ values are observed at all spectral ordinates. Most of the sites in the RESORCE dataset, nevertheless, are located on soft rock sites with $V_{S30} \sim 450$ m/s. Hence, for a site with V_{S30} close to 450 m/s, the $\delta S2S_s$ values are generally close to zero at all periods. This is the case for Site #2 with $V_{S30} = 480$m/s, in which the site-term $\varepsilon^{\delta S2S_2} \sim 1.0$ is observed over the broad period range of $T = 0.01$-1.0 s.

Third, and perhaps the most critical aspect of $\delta S2S_s$ in the context of a PSHA, is the issue of nonlinear soil response at these sites - particularly at the stiff soil Site #3. Recording stations at all three sites are located at surface in free-field. Table 1 shows the range of ground-motion prediction (PGA) recorded at these sites from predominantly $M5$-$M6$ earthquakes at 30km$< R_{JB} <$150 km. The values of the $\delta S2S_s$ term estimated from these records are unlikely to have included any significant nonlinear soil behavior. However, typical ruptures considered in PSHA in most parts of the world include also much larger earthquakes at much closer distances, scenarios capable of triggering strong nonlinear soil response. In this study, we discounted nonlinear soil response for two reasons:

1. Given the limited evidence of significant soil nonlinearity in RESORCE ground-motion data, the B14 and K16 GMPEs developed from this dataset have not explicitly included a nonlinear soil response term. For example, the Akkar et al. (2014a) GMPE included a globally calibrated, semi-empirical, nonlinear soil response model developed by Sandıkkaya et al. (2013). According to this model, nonlinear soil response for sites with $V_{S30} \geq 339$m/s may occur, albeit in a very limited way and with large uncertainty. Seyhan and Stewart (2014) proposed a semi-empirical nonlinear soil response model based on empirical data from NGA-West2 and one-dimensional (1D) ground response analysis (GRA) by Kamai et al. (2014). This model suggests that, for an input rock ground motion of $PGA_{rock} = 1$g, the V_{s30}-based nonlinear amplification would be approximately 30% lower than the V_{s3} =-based linear-only amplification at Site #3. However, to apply the same 30% reduction to a $\delta S2S_s$-based amplification cannot be justified without evaluating the additional quantitative and qualitative uncertainties.
2. Nonlinear soil response is strongly dependent on the V_s (shear-wave velocity) profile at the site, and is essentially site-specific, unlike the semi-empirical ergodic models proposed by Sandıkkaya et al. (2013) and Seyhan and Stewart (2014). Despite the various uncertainties involved in a site-specific 1D GRA (Aristizábal et al., 2018), V_s profile at our selected sites are either non existant or simply not publicly available.

On the contrary, a more recent study by Pilz and Cotton (2019) demonstrated that $\delta S2S_s$ of KiK-net sites estimated by Kotha et al. (2018b) are able to capture the complex two-dimensional/three-dimensional (2D/3D) effects on site response. In this regard, although soil nonlinear response is an important phenomenon to be accounted for in PSHA, both the lack of site-specific geotechnical information and the limitations of 1D GRA dissuaded us from including it in our analyses. Again, recall that only Site #3 can be expected to show some soil nonlinearity and only for severe ground motions. Otherwise, the inferences from this study are mostly unaffected.

Figure 2a compares the non-ergodic site-specific response spectra predictions for Site #3 using K16 versus the V_{S3} -based ergodic predictions obtained by B14 for three $[M_w, R_{JB}(\text{in km})]$ earthquake scenarios of [5.0; 10]; [6.5; 25]; and [7.2; 25]. It is evident from this plot that the B14 predictions in $T = 0.01$–1.0 s for Site #3 ($V_{S30} = 339$ m/s) are significantly lower than the empirical site-specific predictions of K16 obtained using its $\delta S2S_s$. Essentially, Site #3 appears to exhibit a site-specific amplification at $T = 0.5$ s, a period observed to be characteristic of Site #3 in Figure 1, much higher than that of other sites with similar V_{S30}. This is typical of

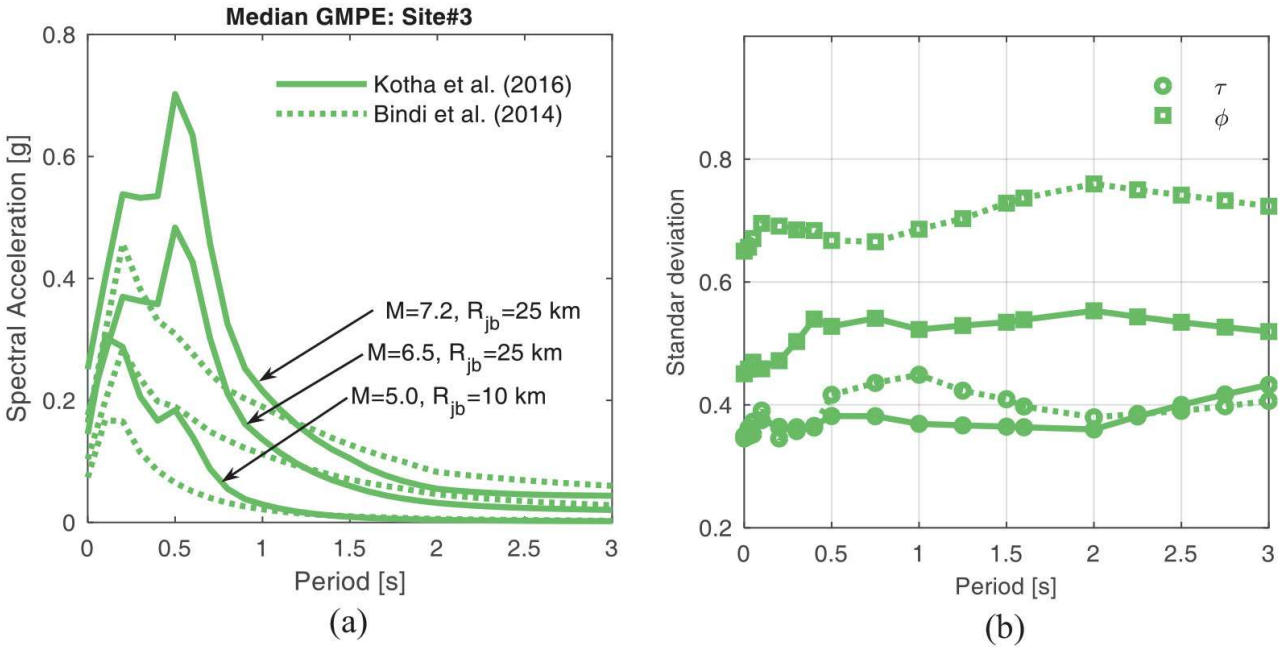

Figure 2. *Comparison of ergodic and non-ergodic site-specific median response spectra at Site #3 for three ([M_w; R_{JB} (in km)]) earthquake scenarios. (b) Standard deviation. Solid lines represent the non-ergodic cases while dotted lines the ergodic cases. The quantities τ and ϕ represent the between-event and within-event error terms, respectively.*

ergodic GMPEs which do not capture the site-to-site response variability among sites with identical V_{S30}. Although not shown here, with a similar reasoning, one can deduce that non-ergodic site-specific response spectra for Site #1 obtained from K16 would be lower than the B14 predictions, while those for Site #2 would be nearly identical. In summary, our selected three sites represent three examples with higher (Site #3), similar (Site #2), and lower (Site #1) site-specific SA predictions than their respective ergodic predictions.

Figure 2b compares the between-event (τ) and within-event (ϕ) standard deviations of the two GMPEs. At short and long periods ($T < 0.5$ s and $T > 1.5$ s), the two GMPEs have very similar values. While in the $T =$ 0.5-1.5 s range, K16 has a smaller t as a result of removing (in the GMPE regression) the $M_w \leq 5$ events with incorrect magnitude estimates. More importantly, ϕ is about 50% smaller for K16 compared with B14. The ϕ of K16 is filtered for site-to-site variability (ϕ_{S2S}) as well, making it ~50% lower than that of B14. The benefit of moving from ergodic to site-specific GMPEs is, therefore, two-fold: (1) the improved accuracy of median estimates because of using $\delta S2S_s$ (and thus bias removal) and (2) the improved precision because of reduced dispersion, that is, the smaller ϕ. The compounded impact on PSHA was demonstrated for 225 sites in pan-European region by Kotha et al. (2017a). The present study will go a step further and show the impact of using site-specific GMPEs on risk estimates for structures at the three selected sites.

Probabilistic seismic hazard analysis

For the three selected sites with the metadata provided in Table 1, we performed PSHA with OpenQuake™ (Pagani et al., 2014) using the SHARE area-source seismic hazard model (Woessner et al., 2015), and the two GMPEs of B14 and K16. The PSHA approach based on B14 is referred to as ergodic hereinafter. It follows the classical integration method (Cornell, 1968) which is a "soil-specific but site generic" PSHA approach, because the GMPE relies on V_{S3} - a soil-specific stiffness proxy. But the amplification at the surface of any specific soil deposit with a given V_{S30} is derived from seismograms recorded at several sites with identical V_{S3}, assuming their site-response to be identical as well, hence, ergodic. On the contrary, the PSHA approach (Kotha et al., 2017a) using K16 (without V_{S30}) is referred to as non-ergodic in this paper. This non-ergodic approach can be considered as a "site-and-soil-specific" PSHA instead, because the hazard curves for a site are obtained using the site term $\delta S2S_s$, which is derived from the seismograms at that specific site - disregarding any V_{S30} information at the site. In essence, the $\delta S2S_s$ term accounts for the effects of the site as a whole, including that due to the soil deposit.

Figure 3a to c compares the hazard curves obtained from non-ergodic approach (dotted lines) and ergodic approach (solid lines) for SA(0.2 s), SA(0.5 s), and SA(1.0 s) at the three sites, respectively. The colored ribbons

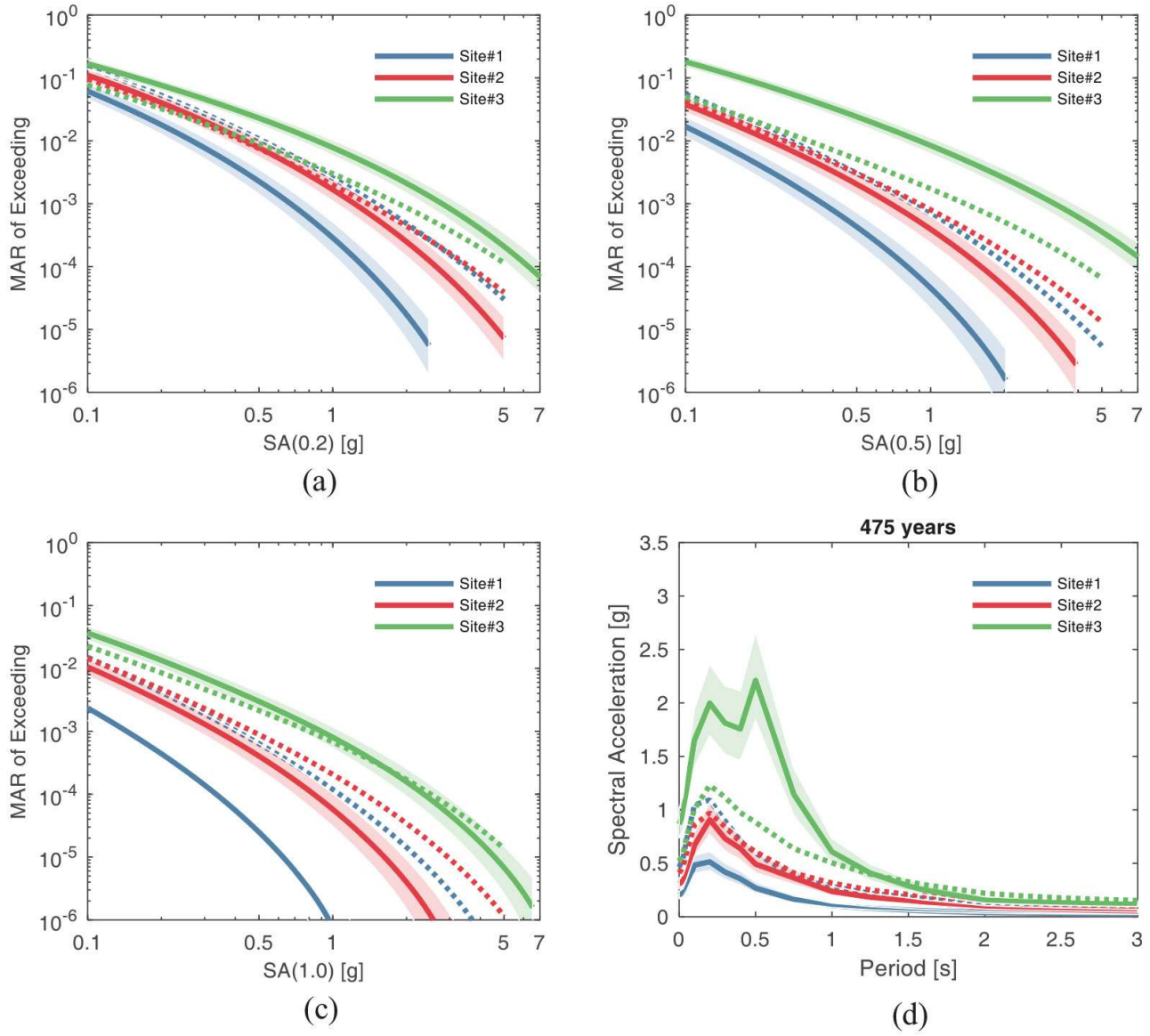

Figure 3. *Comparison between the ergodic and non-ergodic results of PSHA for the three selected sites. (a) Hazard curves for SA(0.2 s). (b) Hazard curves for SA(0.5 s). (c) Hazard curves for SA(1.0 s). (d) Uniform hazard spectra (UHS) for 10% probability of exceedance in 50 years. Solid lines represent the results of the non-ergodic PSHA and the dotted lines are obtained from the ergodic approach. The colored ribbon indicates the uncertainty in the estimates of* $\delta S2S_s$ *due to the limited number of records at the site.*

around the non-ergodic hazard curves reflect the uncertainty in the ground motion at any hazard level as a consequence of uncertainty on the estimates of $\delta S2S_s$, due to the small sample of seismograms recorded at the site. The differences between soil-specific (ergodic) and site-specific (non-ergodic) hazard curves stem from using both the site-specific $\delta S2S_s$ term instead of the soil-specific V_{S30}, and the reduced site-specific GMPE s (Figure 2b). The contribution of $\delta S2S_s$ to the differences is expected across the entire MAR range (Kotha et al., 2017a) because it is a scenario-independent scaling factor, while that of reduced σ is more prominent at lower MAR values (Bommer and Abrahamson, 2006).

Figure 3d compares the non-ergodic and ergodic uniform hazard spectra (UHS) at 475 years return period (i.e. 10% probability exceeding in 50 years) for the three sites. Once again, the differences in the UHS obtained from the two approaches can be explained with reference both to the site terms $\delta S2S_s$ shown in Figure 1b, and to the lower s of nonergodic GMPE from omitting site-to-site aleatory variability ϕ_{S2S}. However, at the 475 years return period (MAR~2×10^{-3}) level, the effect of reduced σ on PSHA is not as drastic as it is at longer return periods, for example, at 10,000 years (MAR~10^{-5}). Therefore, the differences seen here in the 475-year UHS are primarily from using site-specific $\delta S2S_s$ instead of V_{S30} to account for the site response. Needless to say, the differences between ergodic and non-ergodic UHS vary with the return period. For Site #3, despite

the reduced non-ergodic σ, the non-ergodic 475-year UHS is significantly above its ergodic counterpart around $T = 0.5$ s, because its site-specific $\delta S2S_s$ shows a strong amplification peak around $T = 0.5$ s. The differences, however, are negligible at $T = 1$ s and longer periods, because the $\delta S2S_s$-based amplification values at longer periods are close to those predicted by V_{S30}, as seen in Figure 2a.

On the contrary, for Site #1, the significantly lower non-ergodic 475-year UHS is due to its low $\delta S2S_s$, which suggests that the empirical site-specific amplification is lower than that predicted using its V_{s3} by the B14 GMPE. Traditionally, hazard curves at a site or hazard maps containing thousands of sites are estimated for reference rock conditions, which in pan-European region is $V_{S3} = 800$m/s. Hence Site #1, with its $V_{S30} = 747$m/s, should resemble a typical reference rock site; yet there is a large difference between its ergodic and non-ergodic hazard estimates. This result revisits a well-known question of whether V_{S30} is a sufficient site-response proxy for reference site conditions, and supports as well our suggestion to pursue site-specific hazard and risk assessments, whenever possible. Unfortunately, not enough geotechnical information is available in the RESORCE dataset to further characterize and explain the deviation of this site's behavior from expected reference rock conditions.

For Site #2, the ergodic and non-ergodic hazard curves nearly coincide at low hazard levels (high MAR), but significantly deviate at high hazard levels (low MAR), solely because of the reduced non-ergodic σ. This means that, although the two 475-year UHS are very similar, at longer return periods the non-ergodic UHS would be lower than the ergodic UHS due to the lower non-ergodic σ. Our choice of these three well-sampled sites in Turkey was made so that their $\delta S2S_s$ have low epistemic uncertainties, and they fall into three different Eurocode 8 soil classes. The site-specific amplification functions (shown in Figure 1b) portray their uniqueness within their respective Eurocode 8 classes.

Subsequently, we performed an $[M_w, R_{JB}, \varepsilon]$ disaggregation of hazard to identify the controlling (modal) scenarios at different levels of ground-motion intensity. Although not shown here (provided in the Supplementary Material), the disaggregation results from the ergodic non-ergodic PSHA suggest the same modal ruptures, if not for minor differences arising from the regionalization of anelastic attenuation in K16 and its smaller σ. The modal scenarios identified in this step for all the sites and hazard levels are then used for developing the conditional spectra and subsequent record selections for risk analyses of a suite of SDOF idealized structures placed at the three sites.

Probabilistic seismic risk analysis

We considered elastic-perfectly plastic SDOF systems with initial elastic periods of $T_1 = 0.2$ s, $T_1 = 0.5$ s, and $T_1 = 1.0$ s representing ductile moment-resisting frame buildings with different low to medium heights. We assume here that the results of traditional (here called ergodic) PSHA are directly adopted by engineers to compute the seismic design loads for new buildings. This assumption is strictly valid in some codes such as Italian seismic design code (NTC, 2008) and only approximately valid in others, such as ASCE 7 (Structural Engineering Institute, 2006), where the design loads are somewhat derived from PSHA results. As such, we designed the lateral strength of the SDOFs using the 10% in 50 years UHS of the site obtained from the ergodic PSHA results. Therefore, the corresponding yield base shear coefficient C_y, that is, the yield base shear F_y normalized by the weight W, numerically equivalent to the yield spectral acceleration SA_y in units of g (i.e. acceleration of gravity), namely, $C_y = SA_y/g = V_y/W$, is obtained by $C_y = SA_{des}(T_1) \cdot \Omega/(q \cdot g)$, where $SA_{des}(T_1)$ is the design spectral acceleration at T_1, q is the behavior factor assumed equal to 4.0 for new ductile buildings, and $\Omega = 2.0$ is the overstrength factor. Accordingly, the corresponding yield displacement, δ_y, of the SDOF is obtained by $\delta_y = SA_y \left[\frac{T_1}{2\pi}\right]^2$. Finally, we assume that the SDOF collapses when an ultimate ductility $\mu_u = 8.0$ is reached.

Multiple stripe analysis (MSA; Jalayer and Cornell, 2009), is performed to estimate the response of the SDOFs using a large database of real ground-motion recordings. This requires multiple nonlinear dynamic analyses at each one of the predetermined IM levels. To accurately capture the site-dependency of the structural response (Kohrangi et al., 2017), appropriate record selection is required at each IM level to provide the link between hazard and structural response. Herein, we utilize the conditional spectrum (CS)-based record selection approach (Jayaram et al., 2011), to select sets of records that best represent the seismic hazard at each site. We consider eight IM levels, corresponding to probabilities of exceedance at 30.0%, 10.0%, 5.0%, 2%, 1.0%, 0.6%, 0.2%, and 0.1% in 50 years. The conditioning IM, called here IM^*, of choice is the 5% damped geometric mean SA of the two horizontal components, $SA(T^*)$, at three conditioning periods of $T^* = 0.2$, 0.5,

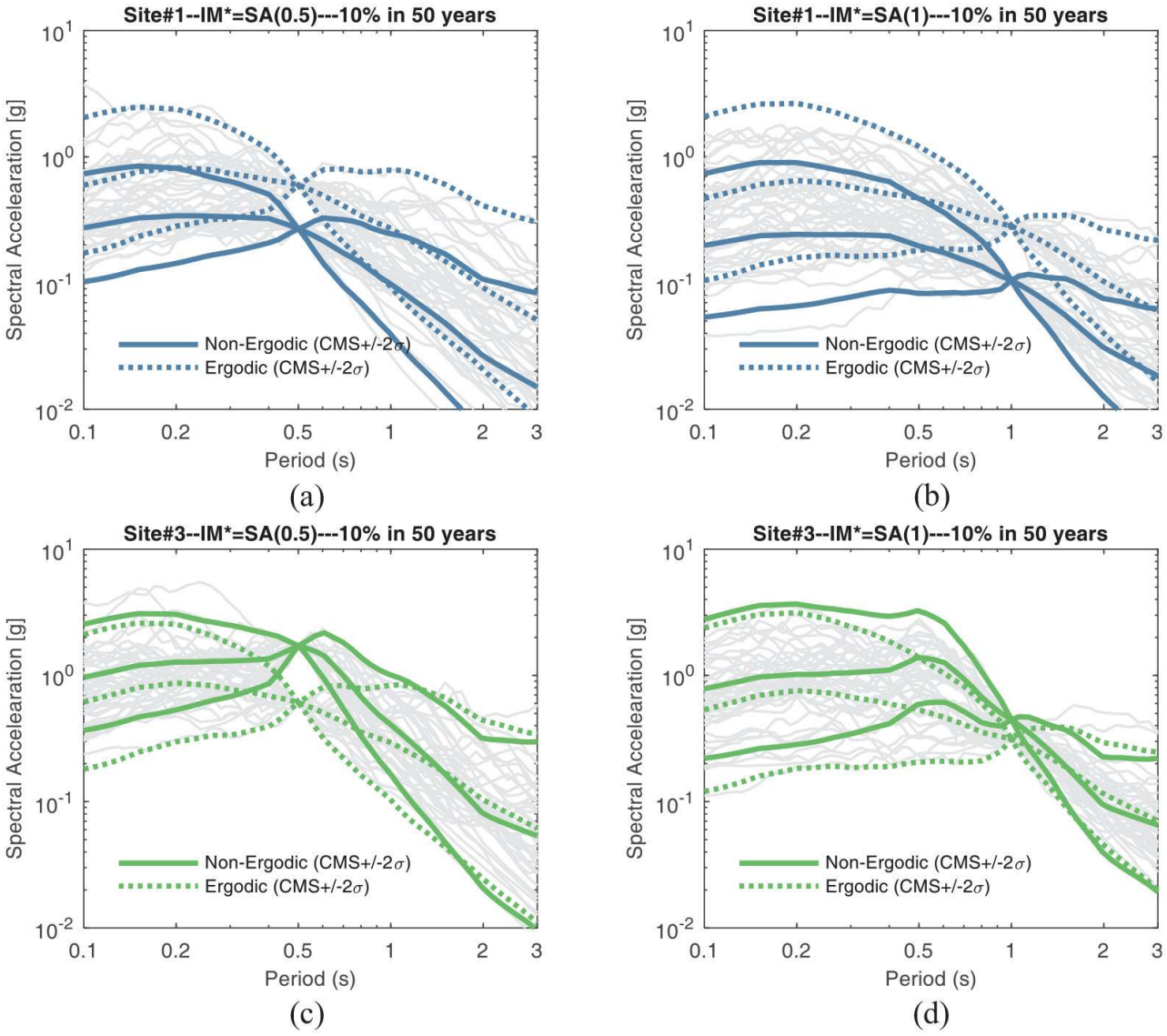

Figure 4. *Comparison of the selected records and the target conditional spectra in terms of the 2.5th; 50th; 97.5th percentiles at 10% in 50 years probability of exceedance for ergodic versus nonergodic approaches corresponding to: (a) $IM^* = SA(0.5\ s)$ at Site #1; (b) $IM^* = SA(1.0\ s)$ at Site #1; (c) $IM^* = SA(0.5\ s)$ at Site #3; and (d) $IM^* = SA(1.0\ s)$ at Site #3. The response spectra of individual selected records are shown in gray.*

and 1.0 s.

The hazard disaggregation results are used to identify modal scenarios contributing to the hazard at each one of the three sites, for three conditioning *IM*s, and at each one of the eight aforementioned *IM* levels. The exact method of CS of Lin et al. (2013) is adopted herein to generate the CS target spectra. For each PSHA method, its corresponding GMPE is also utilized in the CS approach. At *IM* level, 21 records from the PEER NGAWest database (Chiou et al., 2008) are selected and scaled to collectively match the target spectral acceleration mean and variance, leading to suites of 168 ordinary ground-motion recordings (i.e. excluding pulse-like recordings and recordings of ultralong duration caused by subduction zone earthquakes) for three conditioning *IM*s and for the two PSHA approaches. The correlation models utilized in the CS record selection are adopted from Kotha et al. (2017b) using *site and region-independent* correlation model for the ergodic approach and the *site-corrected region and magnitude–dependent* correlation model for the non-ergodic approach. Figure 4 shows, for example, the response spectra of the selected records for Site #1 and Site #3 conditioned on $SA(0.5\ s)$ and $SA(1.0\ s)$ at 10% probability of exceeding in 50 years, as well as the target CS in terms of median plus/minus two standard deviations, that is, "CMS±2σ." Several important issues should be considered when inspecting Figure 4.

First, the analysis that we have called *ergodic* here may have been referred to as "site-specific" in the past

literature. Strictly speaking, this was a misnomer since any ergodic GMPE, here the B14, does not reflect the characteristics of the spectral shape or ground-motion intensity of any specific site, but it was designed to work for a generic site with specific soil conditions, earlier in time, of given NEHRP soil type or, more recently, of given V_{S30}. What we herein call *non-ergodic*, however, is based on a partially non-ergodic site-specific GMPE, here K16, designed to capture any peculiarity of the spectral shape or intensity of the ground motion specific to the site under consideration, including its soil conditions. As such, the second approach embeds a higher level of site-specificity, which is clearly evident from the shape and amplitude differences of the conditional spectra for the same site, IM and return period obtained from the two approaches (Figure 4).

Second, because the ground-motion intensities estimated by the two approaches for the same return period (or IM^* level) are not necessarily equal (see Sites #1 and #3 here) the two sets of CS-based hazard-consistent ground motions do not hinge at the same spectral value. For example, Figure 4a and b shows that the ergodic approach provides larger estimates of the intensity than the non-ergodic one for Site #1, while Figure 4c and d displays the opposite trend for Site #3.

Third, contrary to the ergodic PSHA approach that delivers smooth CS-based target spectra, the non-ergodic approach reflects any peculiarity of the ground-motion spectral shape specific to the site in the CS. For example, as discussed in the context of Figure 1a, the site-term $\delta S2S_s$ of Site #3 showed a sharp peak at $T = 0.5$ s, which is also reflected in the target CS and, consequently, in the selected records whose response spectra are shown in light gray in Figure 4c and d.

Structural response and fragility analysis

This section discusses the nonlinear dynamic analyses based on non-ergodic and ergodic approaches of the three SDOFs located at the three sites. Here, we use the maximum ductility of the SDOFs as the engineering demand parameter (EDP). Figure 5 shows the results of multiple stripe analyses in terms of maximum ductility demands versus the return period of the IM^*s of the three SDOFs. Each one of the eight stripes present two sets of 21 data points corresponding with the ground-motion records selected via the non-ergodic and ergodic approaches. A ground-motion record that produces ductility $\mu_u \geq 8.0$ is treated as a collapse case and its result appear as a dot placed on the dashed horizontal gray line. In Figure 5 the median maximum ductility of adjacent stripes is connected by straight lines (solid for the non-ergodic case and dotted for the ergodic one). Note that for stripes with more than 50% collapsed data points, the median ductility demand is infinite and, thus, omitted in the figure.

While the non-ergodic approach for Site #1 estimates ductility demands for all tested SDOFs at all return periods lower than those of the ergodic approach, Site #3 shows the exact converse. Such trends can be explained by inspecting the differences in ground-motion intensity estimates of these sites based on the two PSHA approaches. For example, at Site #1 the spectral acceleration at $T = 0.5$ s for 10% probability of exceedance in 50 years obtained from the non-ergodic (subscript NE) approach is $SA_{NE,10\%}$ (0.5 s) $= 0.27g$ while the corresponding value based on the ergodic (subscript E) approach is $SA_{E,10\%}$ (0.5 s) $= 0.6g$ (Figure 3b). This comparison for Site #3 for the same hazard level shows, $SA_{NE,10\%}$ (0.5 s) $= 1.72g$ versus $SA_{E,10\%}$ (0.5 s) $= 0.6g$. Site #2, however, exhibits less significant differences in the ductility demands computed by both methods because the hazard estimates are, relatively speaking, closer (i.e. $SA_{NE,10\%}$ (0.5 s) $= 0.63g$ and $SA_{E,10\%}$ (0.5 s) $= 0.88g$ at the 10% in 50-year level) than those computed by the two PSHA methods for the other two sites.

Fragility curves

In regional portfolio seismic risk assessment models often fragility curves for multiple limit states are utilized to assess the risk of different classes of buildings. The fragility curves are then coupled with loss estimates for each limit state (LS) to obtain the so-called vulnerability functions that provide loss estimates for a range of ground-motion intensities. While traditionally these fragility curves are derived independently of the site hazard (namely, using ground-motion records that are not statistically consistent with the hazard at the site), Kohrangi et al. (2017) showed that fragility curves of identical buildings at two distinct sites are indeed site dependent. This was proved by utilizing a CS-based record selection for each site that using a traditional ergodic PSHA. The natural next step would be to follow the site-specific non-ergodic PSHA of the current study to generate site-dependent fragilities and to show that they are not only different from site to site, but also at a given site different from those computed via the ergodic PSHA. As an illustrative example, Figure 6 shows

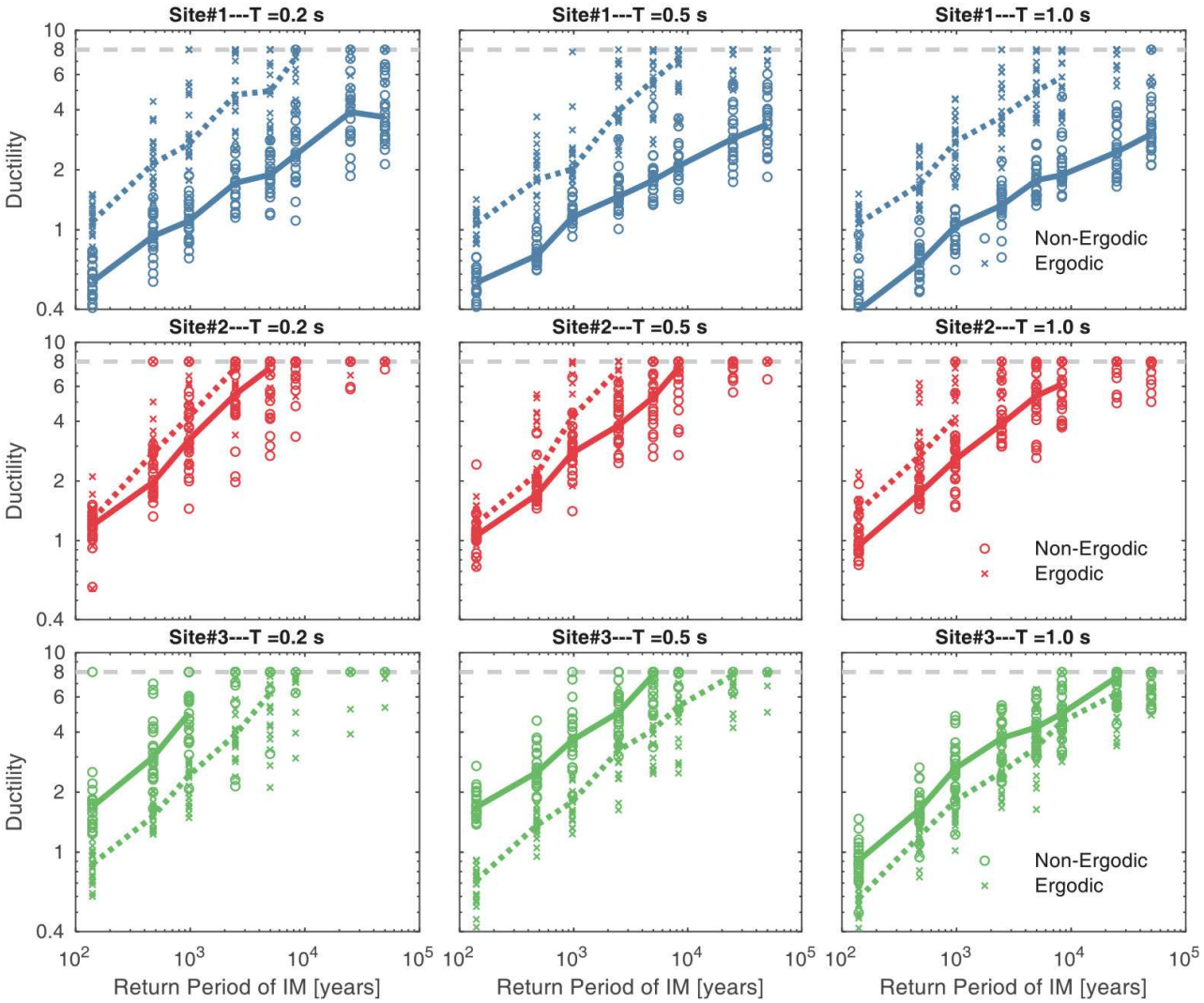

Figure 5. *Comparison of the SDOFs' maximum ductility obtained from soil-specific versus site-specific approaches for the three sites. The solid and dotted lines connect the median maximum ductility values of successive stripes for non-ergodic and ergodic approaches, respectively.*

and compares the fragility curves for the SDOF with $T_1 = 0.5$ s representing the probability of an LS with $\mu_u \geq 3.0$ given $SA(0.5\text{ s})$ for Sites #1 and #3 based on the non-ergodic and ergodic PSHA approaches.

First of all, this figure confirms the findings of Kohrangi et al. (2017) that identical buildings at different sites exhibit different fragility curves. However, this figure lets us also explore the differences among fragility curves for the same SDOF at the same site stemming from using the ergodic and non-ergodic GMPEs. The differences in the fragility curves observed in the cases illustrated in Figure 6 can be explained by the differences of the spectral shapes of the ergodic and non-ergodic CS. The difference in amplitude of two CS from the two PSHA approaches for the same return period has no influence on the fragility curve. Incidentally it will influence, however, the annual probability of reaching or exceeding that LS, as we will see later. As shown in Figure 4a, the target spectral shape of the ergodic and non-ergodic approaches at Site #3 are significantly different for this SDOF system at the 10% in 50 years exceedance level. If the two CS were normalized at the same amplitude of the $SA(0.5\text{ s})$ pinch-point, it would be apparent that the frequency content in the periods of oscillation longer than 0.5 s was higher for the records matched to the ergodic CS, making them more aggressive for the damaged SDOF system oscillating at periods longer than the initial elastic 0.5 s. This translates into a significant overestimation of the probability of exceeding this LS, overestimation that is made evident by an ergodic fragility curve shifted toward the left compared with that of the non-ergodic one. The shape of the non-ergodic CS recognizes that at this site records reach high levels of $SA(0.5\text{ s})$ at a peak of the spectrum that falls sharply at longer periods. This peculiarity of the spectral shape is lost in the smoother ergodic CS. Conversely, at Site #1 where the differences in spectral shape of the two CS are minimal, the fragility curves

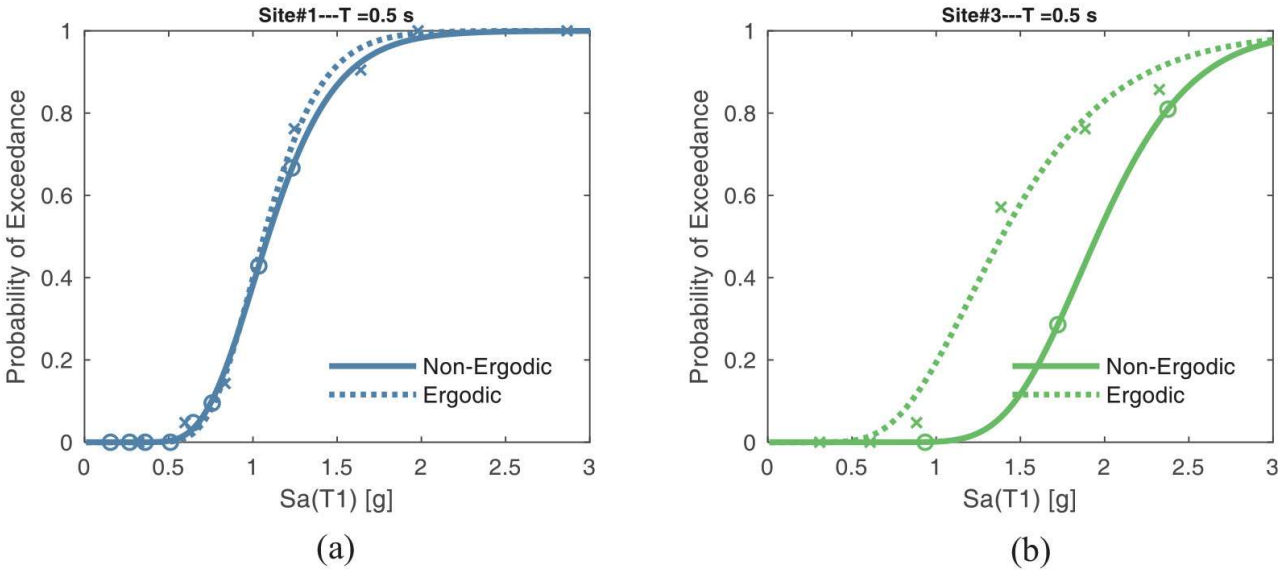

Figure 6. *Comparison between the fragility curves obtained from ergodic versus non-ergodic approaches for an intermediate damage LS defined as $\mu > 3.0$; (a) SDOF with $T_1 = 0.5$ s at Site #1; (b) SDOF with $T_1 = 0.5$ s at Site #3. Solid lines represent the fragility curves obtained using records selected in accordance with non-ergodic hazard estimates while dotted are the corresponding ones based on ergodic PSHA.*

are also essentially indistinguishable.

Response hazard curve and risk of collapse

Following Shome (1999), the annual rate of exceeding different values of an EDP, $\lambda(edp > EDP)$ is computed here. This involves a convolution of the hazard curves of Figure 3 with the response curves in Figure 5. Figure 7 compares the ergodic and the non-ergodic risk estimates, here expressed in MAR of exceeding different ductility levels. These curves represent the output of the risk assessment carried out in this study. Figure 7 shows, as expected, that the risk estimates can be very sensitive to the approach used for performing the PSHA. For each site and SDOF system, the discrepancies between the corresponding ergodic and non-ergodic response hazard curves are primarily explained by the differences in the input ergodic and non-ergodic hazard curves (Figure 3) and, secondarily, by the differences in the response curves (Figure 5) from both approaches.

For example, for the three SDOFs at Site #1, the non-ergodic response hazard curves are significantly lower, although to a different extent across SDOFs, than their ergodic counterparts. The lower hazard estimates carry over to the risk estimates. As referred to above, the second reason for these differences pertains to the two distinct hazard-consistent record selections that affect the structural response (Figure 5). The trend opposite to all the SDOFs at Site #1, applies to the 0.2 s and 0.5 s SDOFs at Site #3, and to the 0.5 s and 1.0 s SDOFs at Site #2 for which the non-ergodic estimates of the risk are higher than the traditional ergodic ones. This happens for the same reason explained above. However, the two risk estimates for the 1.0 s SDOF at this site are quite similar mainly because the ergodic and non-ergodic hazard curves are similar, as Figure 3 shows. The likeness of the response hazard curves across approaches applies also to the SA(0.2 s) SDOF located at Site #2 where ergodic and non-ergodic hazard estimates are also similar.

It is evident that the structural risk computed via the more advanced non-ergodic GMPE approach can be higher than, lower than or essentially the same as the traditional risk estimates computed utilizing ergodic GMPEs. In addition, the trend may change across SDOF systems located at the same site. However, we can go a step further in our statements and mention possible bias rather than simply talking about discrepancies in risk estimates. We argue that the risk estimates based on the non-ergodic PSHA results can be considered as a sort of benchmark since they are more accurate than the traditional ones. This is because of the specificity of the PSHA calculations to the soil and site under consideration as opposed to the traditional ones that are derived for a soil of a given V_{S30} regardless of the site. The risk estimates based on the traditional ergodic PSHA approach can be (1) conservative (i.e. providing higher rates than the non-ergodic counterpart), as is the case for all three SDOFs at Site #1 here, (2) un-conservative (as is the case for the SA(0.5 s) and SA(1.0 s) SDOF systems at Site #2 and for the SA(0.2 s) and SA(0.5 s) SDOF systems at Site #3 here), or (3) very similar (as for the SA(0.2 s) SDOF at Site #2 and the SA(1 s) SDOF at Site #3). Which one of these three cases one would

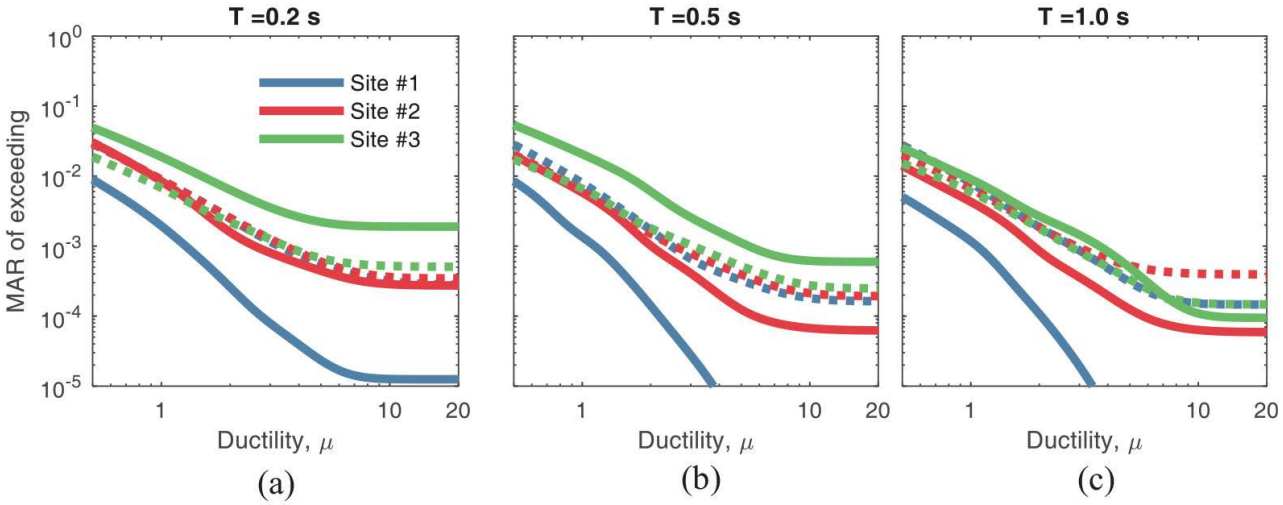

Figure 7. *Comparison between the response hazard curves for the three sites obtained from using ergodic versus non-ergodic PSHA. (a) SDOF with $T_1 = 0.2$ s. (b) SDOF with $T_1 = 0.5$ s; (c) SDOF with $T_1 = 1{:}0$ s. Solid lines represent the non-ergodic case and dotted lines represent the ergodic case.*

encounter in a real application is not obvious without performing also a PSHA that uses a non-ergodic GMPE.

Concluding remarks

This study presented a comparison between the seismic risk estimates obtained from using PSHA-based hazard estimates from two approaches: the traditional one, which uses an ergodic, soil-specific but site-generic GMPE, and one that uses a partially non-ergodic, site-and-soil-specific GMPE. The ergodic GMPE accounts for site effects only as a function of V_{S3} , a proxy for stiffness of the top 30 m of a 1D soil column, disregarding, for example, the deeper soil profile and 2D/3D topographic effects of the specific site where it is applied. Whereas the non-ergodic approach benefits from an empirically estimated site-specific $\delta S2S_s$ term, which appears to capture a variety of geotechnical and geological effects. We note that, nonlinear soil response is discounted from our analysis due to lack of compelling empirical evidence and absence of site-specific V_S profiles for 1D GRA.

The case study presented utilized two comparable GMPEs of Bindi et al. (2014) and Kotha et al. (2016) to perform ergodic and non-ergodic PSHA, respectively, and the SHARE earthquake occurrence model to estimate the seismic hazard at three sites located in Turkey. Then for each site we used the hazard estimates of the two PSHA approaches to select two suites of hazard-consistent ground-motion records that were utilized as input to estimate the response of three ductile buildings of different heights via MSA. Both the difference in site hazard and in the ground motions consistent with the two different views of the site hazard are jointly responsible for the amplitude of the structure-and-site specific response hazard curves, which represent the risk estimates here.

The risk estimates, which are obtained by convolving the response with the site hazard curves, show that the traditional ergodic approach can be conservative, un-conservative, or about right in a way that is impossible a priori to discern without performing a site-specific PSHA that utilizes a non-ergodic GMPE. These results also help in debunking the simplistic (and wrong) idea that the lower standard deviation of non-ergodic GMPEs implies lower hazard and, therefore, lower risk estimates. The amount of bias, also, is not the same for all buildings at a given site but depends on the dynamic characteristic of the building vis-a-vis the dynamic characteristic of the soil at the site.

Although these are very compelling arguments supporting the use non-ergodic GMPEs in risk assessment, it is important to note that this route is feasible only at sites with a sufficient number of ground-motion recordings. This criterion ensures that the epistemic uncertainties (standard errors) are negligibly small compared to the GMPE apparent aleatory variability. In the newer ground-motion datasets, there are literally tens of sites with a sufficient number of recordings each to allow such an approach. With continued effort toward compiling large datasets, risk assessment based on more accurate, non-ergodic hazard assessment could soon become the state of practice.

Acknowledgments
The authors are very thankful to the two anonymous reviewers and the associate editor, Jonathan Stewart, and Editor-in-Chief, David Wald, whose thorough review helped in substantially improving the manuscript.

Declaration of conflicting interests
The author(s) declared no potential conflicts of interest with respect to the research, authorship, and/or publication of this article.

Funding
The author(s) disclosed receipt of the following financial support for the research, authorship, and/or publication of this article: The contributions of S.R.K. (second author) in this research are funded by the SIGMA2 consortium (EDF, CEA, PG&E, SwissNuclear, Areva, CEZ, CRIEPI) under grant – 2017–2021.

ORCID iDs
Mohsen Kohrangi https://orcid.org/0000-0001-9151-0361
Sreeram Reddy Kotha https://orcid.org/0000-0002-4874-3730

Supplemental material
Supplemental material for this article is available online.

References
Akkar S, Sandıkkaya M and Bommer J (2014a) Empirical ground-motion models for point-and extended-source crustal earthquake scenarios in Europe and the Middle East. Bulletin of Earthquake Engineering 12: 359–387.

Akkar S, Sandıkkaya M, Sxenyurt M, Sisi AA, Ay B, Traversa P, Douglas J, Cotton F, Luzi L, Hernandez B and Godey S (2014b) Reference database for seismic ground-motion in Europe (RESORCE). Bulletin of Earthquake Engineering 12: 311–339.

Al Atik L, Abrahamson N, Bommer JJ, Scherbaum F, Cotton F and Kuehn N (2010) The variability of ground-motion prediction models and its components. Seismological Research Letters 81: 794–801.

Ancheta TD, Darragh RB, Stewart JP, Seyhan E, Silva WJ, Chiou BS-J, Wooddell KE, Graves RW, Kottke AR and Boore DM (2014) NGA-West2 database. Earthquake Spectra 30: 989–1005.

Anderson JG and Brune JN (1999) Probabilistic seismic hazard analysis without the ergodic assumption. Seismological Research Letters 70: 19–28.

Aristiza´bal C, Bard P-Y, Beauval C and Go´mez J (2018) Integration of site effects into probabilistic seismic hazard assessment (PSHA): A comparison between two fully probabilistic methods on the euroseistest site. Geosciences 8: 285.

Bazzurro P and Cornell CA (2004) Nonlinear soil-site effects in probabilistic seismic-hazard analysis. Bulletin of the Seismological Society of America 94: 2110–2123.

Bindi D, Massa M, Luzi L, Ameri G, Pacor F, Puglia R and Augliera P (2014) Pan-European ground-motion prediction equations for the average horizontal component of PGA, PGV, and 5%-damped PSA at spectral periods up to 3.0 s using the RESORCE dataset. Bulletin of Earthquake Engineering 12: 391–430.

Bommer JJ and Abrahamson NA (2006) Why do modern probabilistic seismic-hazard analyses often lead to increased hazard estimates? Bulletin of the Seismological Society of America 96: 1967–1977.

Chiou B, Darragh R, Gregor N and Silva W (2008) NGA project strong-motion database. Earthquake Spectra 24: 23–44.

Code P (2005) Eurocode 8: Design of Structures for Earthquake Resistance-Part 1: General Rules, Seismic Actions and Rules for Buildings. Brussels: European Committee for Standardization.

Cornell CA (1968) Engineering seismic risk analysis. Bulletin of the Seismological Society of America 58: 1583–1606.

Jalayer F and Cornell CA (2009) Alternative nonlinear demand estimation methods for probability-based seismic assessments. Earthquake Engineering & Structural Dynamics 38: 951–972.

Jayaram N, Lin T and Baker JW (2011) A computationally efficient ground-motion selection algorithm for matching a target response spectrum mean and variance. Earthquake Spectra 27: 797–815.

Kamai R, Abrahamson NA and Silva WJ (2014) Nonlinear horizontal site amplification for constraining the NGA-West2 GMPEs. Earthquake Spectra 30: 1223–1240.

Kohrangi M, Vamvatsikos D and Bazzurro P (2017) Site dependence and record selection schemes for building fragility and regional loss assessment. Earthquake Engineering & Structural Dynamics 46: 1625–1643.

Kotha SR, Bazzurro P and Pagani M (2018a) Effects of epistemic uncertainty in seismic hazard estimates on building portfolio losses. Earthquake Spectra 34: 217–236.

Kotha SR, Bindi D and Cotton F (2016) Partially non-ergodic region specific GMPE for Europe and Middle-East. Bulletin of Earthquake Engineering 14: 1245–1263.

Kotha SR, Bindi D and Cotton F (2017a) From ergodic to region- and site-specific probabilistic seismic hazard assessment: Method development and application at European and Middle Eastern sites. Earthquake Spectra 33: 1433–1453.

Kotha SR, Bindi D and Cotton F (2017b) Site-corrected magnitude- and region-dependent correlations of horizontal peak

spectral amplitudes. Earthquake Spectra 33: 1415–1432.
Kotha SR, Cotton F and Bindi D (2018b) A new approach to site classification: Mixed-effects ground motion prediction equation with spectral clustering of site amplification functions. Soil Dynamics and Earthquake Engineering 110: 318–329.
Lin T, Harmsen SC, Baker JW and Luco N (2013) Conditional spectrum computation incorporating multiple causal earthquakes and ground-motion prediction models. Bulletin of the Seismological Society of America 103: 1103–1116.
NTC LG (2008) Norme tecniche per le costruzioni [Italian Technical Norms for Constructions]. Available at: http://www.ingegneriasoft.com/NTC2008_Norme_tecniche_per_le_costruzioni.htm
Pagani M, Monelli D, Weatherill G, Danciu L, Crowley H, Silva V, Henshaw P, Butler L, Nastasi M, Panzeri L, Simionato M and Vigano D (2014) OpenQuake Engine: An open hazard (and risk) software for the global earthquake model. Seismological Research Letters 85: 692–702.
Pilz M and Cotton F (2019) Does the one-dimensional assumption hold for site response analysis? A study of seismic site responses and implication for ground motion assessment using KiK-Net strong-motion data. Earthquake Spectra 35: 883–905.
Rathje E, Pehlivan M, Gilbert R and Rodriguez-Marek A (2015) Incorporating site response into seismic hazard assessments for critical facilities: A probabilistic approach. In: Ansal A and Sakr M (eds) Perspectives on Earthquake Geotechnical Engineering. New York: Springer, pp. 93–111.
Rodriguez-Marek A, Cotton F, Abrahamson NA, Akkar S, Al Atik L, Edwards B, Montalva GA and Dawood HM (2013) A model for single-station standard deviation using data from various tectonic regions. Bulletin of the Seismological Society of America 103: 3149–3163.
Sandıkkaya MA, Akkar S and Bard PY (2013) A nonlinear site-amplification model for the next pan-European ground-motion prediction equations. Bulletin of the Seismological Society of America 103: 19–32.
Scheingraber C and Ka¨ ser MA (2019) The impact of portfolio location uncertainty on probabilistic seismic risk analysis. Risk Analysis 39: 695–712.
Seyhan E and Stewart JP (2014) Semi-empirical nonlinear site amplification from NGA-West2 data and simulations. Earthquake Spectra 30: 1241–1256.
Shome N (1999) Probabilistic Seismic Demand Analysis of Nonlinear Structures. Stanford, CA: Stanford University.
Stafford PJ (2014) Crossed and nested mixed-effects approaches for enhanced model development and removal of the ergodic assumption in empirical ground-motion models. Bulletin of the Seismological Society of America 104: 702–719.
Stewart JP, Afshari K and Goulet CA (2017) Non-ergodic site response in seismic hazard analysis. Earthquake Spectra 33: 1385–1414.
Structural Engineering Institute (2006) Minimum Design Loads for Buildings and Other Structures, Vol. 5 and 7. Reston, VA: American Society of Civil Engineers.
Villani M and Abrahamson NA (2015) Repeatable site and path effects on the ground-motion sigma based on empirical data from southern California and simulated waveforms from the CyberShake platform. Bulletin of the Seismological Society of America 105: 2681–2695.
Weatherill G, Kotha SR and Cotton F (2020) Re-thinking site amplification in regional seismic risk assessment. Earthquake Spectra 36(S1): 274–297.
Weatherill G, Silva V, Crowley H and Bazzurro P (2015) Exploring the impact of spatial correlations and uncertainties for portfolio analysis in probabilistic seismic loss estimation. Bulletin of Earthquake Engineering 13: 957–981.
Woessner J, Laurentiu D, Giardini D, Crowley H, Cotton F, Grünthal G, Valensise G, Arvidsson R, Basili R, Demircioglu MB, Hiemer S, Meletti C, Musson RW, Rovida AN, Sesetyan K and Stucchi M (2015) The 2013 European Seismic Hazard Model: Key components and results. Bulletin of Earthquake Engineering 13: 3553–3596.